PB: ~~Large-Scale Clustering of Tropical Precipitation and its Implications for the Radiation Budget across Timescales~~ Large-Scale Clustering of Tropical Precipitation in Interannual Variability and in a Warming Climate: Mechanisms and Implications for the Radiation Budget

P. Blackberg[1,2], M. S. Singh[1,2]

[1]School of Earth, Atmosphere, and Environment, Monash University, Victoria, Australia
[2]Centre of Excellence for the Weather of the 21st Century, Monash University, Victoria, Australia

Corresponding author: P. Blackberg, carlphiliposcar@gmail.com

Abstract

The spatial organization of deep convection in tropical regions is posited to play an important role in determining characteristics of the tropical climate such as the humidity distribution and cloudiness and may therefore be an important control on climate feedbacks. This study analyzes one aspect of convective organization, the clustering of heavy precipitation on large scales, in both interannual variability and under warming in future climate projections. Both observations and global climate models indicate that large-scale clustering is sensitive to the SST gradient in the Pacific, being largest during El Niño events. Under future warming, models project an increase in clustering with a large intermodel spread. The increase is associated with a narrowing of the intertropical convergence zone, while the model spread is partially explained by differences in projections of the SST gradient in the Pacific. Both observations and models indicate large-scale clustering influences the cloud and humidity distributions, albeit with some differences. However, the intermodel spread in changes in clustering with warming is not related to the intermodel spread in projections of tropical-mean relative humidity or low cloudiness in regions of descent, precluding attempts to provide an observational constraint on feedbacks or climate sensitivity. Nevertheless, the tendency for a meridional contraction of precipitation explains about 45% of the variance in projected drying, highlighting the narrowing of the ITCZ as an important aspect of large-scale convective organization in a warmer climate.

Plain Language Summary

The spatial distribution of rainfall in the tropics is expected to change in a warming climate, with potentially important impacts on how much radiation is absorbed by water vapor and reflected by clouds. This study shows that heavy rainfall tends to move towards the equator and to the Pacific Ocean in projections with global climate models, resulting in an overall increase in the "clustering" of rainfall on the large scale. Further, the results show a shift in rainfall to the equator with global warming is associated with a drying of the tropical atmosphere, which may have an influence on how much the planet warms for a given CO_2 change. However, similar observed shifts in rainfall in the current climate are not found to have the same effect on humidity and clouds as for changes with warming, suggesting caution should be exercised when using relationships derived from observations to predict future changes.

1 Introduction

The spatial organization of deep convection in tropical regions plays a critical role in shaping the hydrological cycle and the moisture and cloud distribution (**?**). Changes in organization with warming may therefore have implications for a range of climatic processes, including precipitation extremes (e.g., **???**) and the radiative feedbacks that control equilibrium climate sensitivity (ECS) (e.g., **???**). However, because many of the relevant small-scale processes are not resolved in climate models, it remains unclear how convective organization will evolve in a warmer climate.

While there are numerous ways by which convection may organize, one important mechanism is the clumping or clustering together of convective elements (e.g., **???**). Such clustering occurs on a range of scales (**?**), including at large scales that are resolved by climate models and at mesoscales that can typically only be resolved in high-resolution storm-resolving simulations. Recently, **?** showed that the extent to which tropical precipitation exhibits clustering on the large scale increases with warming in climate projections from the Coupled Model Intercomparison Project phase 5 (CMIP5). This large-scale clustering is distinct from other types of organization on the mesoscale, but idealized simulations suggest that similar processes may act at both scales, and that both large-scale and mesoscale organization of convection may modulate the radiation budget (**?**).

Here we build on the work of **?**, showing that increased clustering of heavy precipitation with warming is a robust feature of the more recent CMIP6 as well as CMIP5. Further, we explore the mechanisms that lead to large-scale clustering of precipitation in the tropics and the influence of an increase in clustering on properties of the atmosphere that are important for the radiation budget. The analysis will compare how clustering varies across different timescales, from interannual variability in both models and observations to changes in the climatological clustering of convection in a warming climate. This approach allows us to assess whether observational constraints of convective organization under current climate conditions can help constrain changes in organization and the associated radiative feedbacks with warming.

Previous studies have highlighted observed relationships between convective organization and the tropical radiation budget (**???**). For example, **?** find tropical mesoscale convective organization and Estimated Inversion Strength (EIS) in subsidence regions are the two strongest predictors of deseasonalized monthly anomalies in net top-of-atmosphere radiation, together explaining about 60 percent of the variance. While the two predictors are significantly correlated and potentially partly mechanistically connected (**?**), the authors find that both have an independent contribution in influencing the tropical radiation budget; EIS is found to have a stronger correlation with the cloudy component of the radiation budget while convective organization is found to have a stronger connection to the clear-sky component of the radiation budget. **?** argue that clustering of deep convective elements is associated with a tropical-mean drying, resulting in increased outgoing longwave radiation due to a reduction in the greenhouse effect. This hypothesis is supported by idealized studies of convective "self-aggregation" (e.g., **?**). Both cloud-resolving and climate-model simulations run in idealized settings reminiscent of tropical conditions (i.e., low rotation rate and weak temperature gradients) show increased outgoing longwave radiation when convection is more clustered within the domain (**?**).

The preceding studies suggest that increased clustering of convection with warming may lead to a negative clear-sky feedback from clustering-induced drying, resulting in reduced equilibrium climate sensitivity (ECS) (**?**). However, recent research suggests that clustering of deep convection on the large scale may also be indirectly connected to a positive shortwave feedback on warming through changes in low clouds (**?**). According to this argument, drying associated with increased clustering of convection is controlled by the large-scale overturning circulation and is most pronounced in regions of climatological descent where low-cloudiness is sensitive to changes in relative humidity. The associated cloud changes then lead to a net positive feedback.

As the above discussion highlights, an important control on convective organization at both large- and mesoscales comes from large-scale circulation patterns, including the Intertropical Convergence Zone (ITCZ), the South Pacific Convergence Zone (SPCZ), the Walker circulation, and convectively-coupled tropical waves (**?????**). Changes to the clustering of precipitation under warming may therefore be linked to, for example, a "narrowing" of the ITCZ due to constraints on the export of energy by the Hadley cell (**?**) or changes in the Walker circulation driven by changes in zonal SST gradients (**?**), which may be associated with "El Nino-like" shifts in the SST climatology (**?**).

In this study we explore how the spatial distribution of heavy precipitation changes with increased large-scale clustering, demonstrating the importance of both meridional contractions and zonal shifts in convection. We further show that the effect of large-scale clustering on low clouds and moisture—key variables that control the radiation budget—varies with timescale and between global climate models and observations, making it difficult to apply constraints from observed variability to a warmer climate. The paper is structured as follows. First we describe the datasets used and our quantification of large-scale clustering of precipitation (Section 2). Then we present the geographical spatial patterns of heavy precipitation that are associated with a high level of clustering (Section 3). After that, we connect the spatial patterns to leading mechanisms driving clustering (Section 4). Finally, we present the moisture and low-cloud distribution associated with clustering (Section 5). Section 6 gives a summary of the key findings and an outlook for future research.

2 Data and Methods

Our analysis is focused on variations in the large-scale clustering of heavy precipitation in the tropics and its relationship to the atmospheric state in both observations and an ensemble of global climate models (GCMs) primarily from CMIP6. We begin by describing the datasets (both model and observational) used, before we describe the quantification of large-scale clustering, and our analysis framework.

2.1 Models

We use simulations from 27 GCMs from CMIP6 (**?**), using data from the years 1970-1999 in the historical scenario, representing the current climate, and from the years 2070-2099 under the Shared Socioeconomic Pathway 585 (SSP5-8.5), representing a warmer climate. The models are chosen based on availability of the required variables and are shown in Figure **??**. We use one ensemble member from each model.

In addition to the CMIP6 models, we also consider a simulation using a high-resolution GCM referred to here as IFS_9_FESOM_5 (**?**). The Deutsches Klimarechenzentrum (DKRZ) Next Generation Earth Modelling Systems (NextGEMS) pre-final cycle provides high-resolution globally simulated atmospheric and oceanic variables for SSP3-7.0 forcing between 2025-2049 using the ECMWF Integrated Forecasting System (IFS) at ∼9 km horizontal grid spacing for the atmosphere and the Finite-VolumE Sea Ice-Ocean model version 2 (FESOM2) at 5 km horizontal grid spacing for the ocean (**?**). Although the model is at high resolution compared to the CMIP6 models, it retains a convection parameterization, and we therefore describe it as a GCM rather than a storm-resolving model. Because the climate change signal during the simulation is small, we only use the high-resolution GCM to characterize interannual variability, using all available years.

2.2 Observations

Observed clustering of tropical precipitation is quantified based on daily precipitation estimates from the National Oceanic and Atmospheric Administration Global Precipitation Climatology Project (NOAA-GPCP) (**?**), using the method described in the next subsection. We further use NOAA-GlobalTemp (**?**), and Clouds and the Earth's Radiant Energy System (CERES) data (**?**) to provide observational estimates of surface temperature and outgoing longwave radiation, respectively. Estimates of vertical pressure velocity and specific and relative humidity are taken from the fifth generation of the European Centre for Medium-Range Weather Forecasts reanalysis (ERA5) (**?**). Apart from precipitation, all variables are taken as monthly averages.

Finally, we develop a simple estimate of the low-cloud fraction using the tropical weather states defined in **?** based on data from the International Satellite Cloud Climatology Project (ISCCP) (**?**). **?** used a clustering algorithm to categorize histograms of cloud-top pressure and optical thickness given by the ISCCP D1 dataset into a series of weather states defined in three hourly polar-orbiting satellite scans with daily global coverage on a $1^\circ \times 1^\circ$ grid. Each weather state is characterized by a histogram in cloud-top pressure and optical thickness that represents the centroid over all members of that weather state. Here we estimate the cloud fraction as a function of pressure for a given weather state as the total frequency of clouds of all optical thicknesses in a given range of cloud-top pressure within the corresponding centroid histogram. We then calculate the low-cloud fraction LCF_i of weather state i as the total cloud fraction below 600 hPa. The monthly low-cloud fraction is taken as

$$LCF = \sum_i f_i LCF_i, \tag{1}$$

where f_i is the frequency of weather state i over the month in question.

As described further below, all observational datasets are regridded conservatively to a common 2.8° × 2.8° grid for analysis. We use observations covering the time period between 1998-2023 for all datasets, except for cloud fraction (based on ISCCP), which is limited to 1998-2017.

2.3 Quantifying Large-Scale Clustering of Heavy Precipitation

We quantify clustering of precipitation following **?** using daily surface precipitation in the tropics (30°S-30°N). To facilitate the comparison of clustering across different models and the observations, we first interpolate the daily precipitation to a 2.8°× 2.8° grid using a first-order conservative method (**?**) to preserve tropical-mean properties from the native grid. Next we define heavily precipitating regions as gridboxes for which the precipitation rate exceeds a threshold. The threshold is calculated as the 95th spatial percentile of daily precipitation over all gridboxes in the tropics temporally averaged over the 30-year climatology (or 25-year in the case of observations). For the GPCP observations, this threshold is 16 mm day^{-1}. Distinct heavy precipitation features are identified as 8-connected contiguous regions of precipitation exceeding the threshold or single grid boxes if there are no neighboring connections.

We define our primary measure of clustering, A_m, as the mean area of heavy precipitation features over the entire tropics. A_m conceptually captures clustering by distinguishing scenes with many small precipitation features and scenes where precipitation is aggregated into fewer and/or larger precipitating features (Figure **??**). The mean area of features, A_m, was chosen due to its interpretability, however, we note that it is only one aspect of the large-scale organization of precipitation, and A_m does not describe important spatial characteristics such as the total area, shape, proximity, gradients of precipitation intensity, and location of precipitation features. A number of other measures of large-scale clustering are analyzed and their interrelationship is presented in Figures S1-4 in the supporting information.

An important aspect of our method is that, by definition, regions of heavy precipitation occupy 5% of the domain on average. Thus when comparing two climates, the mean area fraction of heavy precipitation $\overline{A_f}$ remains constant. Differences in the mean area of features, A_m, between climates are entirely due to a reorganization of precipitation, and changes in A_m are inversely related to the mean number of precipitation features. However, the above constraint does not apply to the precipitation distribution during a given month. Indeed, as we shall see, an important driver of variations in tropical precipitation clustering in interannual variability is the area fraction of precipitation, A_f. We therefore consider the behavior of both the mean area of heavy precipitation features, A_m, and the area fraction of heavy precipitation, A_f, in our analysis below.

2.4 Describing Relationships to Large-Scale Clustering of Heavy Precipitation

Having quantified large-scale precipitation clustering, we seek to characterize the relationships between such clustering and other large-scale climate variables. Specifically, we consider these relationships for interannual variability in both models and observations, and for changes in climate across the CMIP6 ensemble. Throughout, we define interannual variability in a given variable by deseasonalized monthly anomalies, calculated as the monthly-mean anomaly from the climatology of the associated month after detrending the time series. The trend is estimated by a first-order linear least squares regression of the data at each location from the the daily (precipitation-based metrics) or monthly (all other metrics) time series.

As we will see, for interannual variability, the mean area of features, A_m, and the area fraction of precipitation, A_f, are strongly correlated with each other and to the large-scale climatic state. To estimate the individual effect of A_m, we apply the method of Pearson partial correlation (**?**). The partial correlation $r(X, Y|Z)$ represents the relationship between variables X and Y after the removal of the effect of Z, and is given by

$$r(X, Y|Z) = \frac{r(X, Y) - r(X, Z)r(Y, Z)}{\sqrt{1 - r^2(X, Z)}\sqrt{1 - r^2(Y, Z)}}, \tag{2}$$

where $r(X, Y)$ is the regular correlation between X and Y. The significance of partial correlations is evaluated using the standard t-test for partial correlations.

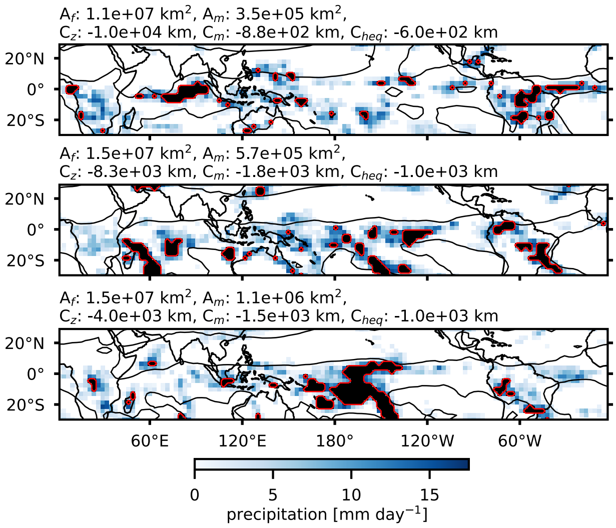

Figure 1. February daily snapshots of GPCP precipitation (blue colors) and regions of heavy precipitation (black shading) with monthly contour of ERA5 500 hPa relative humidity representing the median over the tropics (black line) and monthly ISCCP low cloud fraction (red colors). The panel titles show the total area of heavy precipitation as a fraction of the tropical domain area (A_f), the mean area (A_m) and number (N) of heavy precipitation features, and the Oceanic Niño Index (ONI) taken from NOAA-GlobalTemp. From (a-c), clustering increases according to A_m. The clustering from (a-b) is primarily due to an increase in A_f, whereas the clustering from (b-c) is primarily due to the closer proximity of heavy precipitation to the central Pacific.

3 Spatial Patterns of Heavy Rainfall Clustering

The purpose of this section is to elucidate the spatial patterns of precipitation that produce a high degree of clustering. We first consider how clustering changes in interannual variability before we investigate the spatial patterns associated with strong increases in clustering with warming across the CMIP6 ensemble.

Figure **??** shows the regression of monthly anomalies in the frequency of occurrence of heavy precipitation, C, onto the mean area of heavy precipitation features, A_m, for the observations. When tropical precipitation is observed to be highly clustered on the large scale, heavy precipitation tends to occur more frequently in the central equatorial Pacific. Figure **??** is calculated for all months, but similar spatial patterns can be seen in individual months, strongest in DJF (Figure S5 in the supporting information). Other notable spatial characteristics of the regression include a decrease in heavy precipitation over the maritime continent and a small but statistically significant (crosses) decrease in heavy precipitation over the Amazon and Atlantic.

To quantify the shift of heavy precipitation to the central equatorial Pacific, we define the distance metrics C_z, which represents the mean distance of heavily precipitating points within the tropics to the meridian given by the longitude 180°E, and C_m, which represents a similar metric defined based on distance to the equator. These are somewhat arbitrary zonal and meridional reference lines with which to describe the zonal and meridional shifts, and the clustering redistribution of heavy precipitation may be better characterized relative to the climatological distribution. For example, in most models, with warming heavy precipitation moves south relative to the northern hemisphere climatological convergence zone or north relative the climatological SPCZ or both. However, for simplicity, we use C_z and C_m defined based on 180°E and the equator.

As expected from the regression map, there is a strong relationship between the mean area of features, A_m, and C_z (Figure S2 in the supporting information). However, as shown in Figure **??**a, there is also a strong observed relationship in interannual variability between A_m and the total area fraction of heavy precipitation, A_f [$r^2(A_f, A_m) \sim 0.7$], with greater A_f favoring greater A_m. This suggests a large part of the observed regression pattern is due to the effect of changes in the total precipitating area, rather than a pure spatial redistribution of a fixed number of heavily precipitating points. This complicates the interpretation of increased clustering in internal variability, since when comparing climates, the mean area fraction of heavy precipitation $\overline{A_f}$ remains fixed at 0.05. To address this, we estimate the variations in the distribution of heavy precipitation that contribute to variations in A_m independent of changes in A_f using Pearson partial corelation (see Methods).

Both C_z and C_m are negatively correlated with the mean area of heavy precipitation features, A_m, when the effect of changes in the area fraction of heavy precipitation, A_f, is removed (star in Figure **??**b), suggesting that there is a shift of convection toward the equator and the central Pacific when the tropics are highly clustered. For a given A_f, this contraction of heavily precipitating regions explains about 5-10 percent of the remaining variance after the effect of changes in A_f is removed.

Both the CMIP ensemble and the high-resolution model generally show similar spatial patterns associated with increasing large-scale clustering (Figure **??**b and Figure S6a-b in the supporting information). All models show significant relationships between A_m and A_f, although generally somewhat weaker than in observations, and most models show significant negative partial correlations between the distance metrics C_z (24/27 CMIP6 models) and C_m (22/27 CMIP6 models) after removing the effect of changes in A_f (Figure **??**b). That is, as for the observations, most models agree that higher clustering, as measured by a larger mean area of heavy precipitation features, is associated with a shift in convection toward the central equatorial Pacific. Interestingly, the high-resolution GCM did not show a significant partial correlation with C_m, suggesting clustering in that model is not sensitive to the meridional contraction of heavy precipitation to the equator.

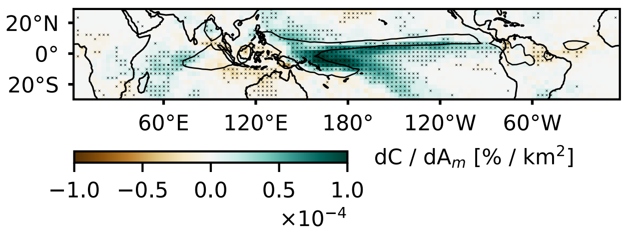

Figure 2. GPCP frequency of occurrence of heavy precipitation, C, regressed onto the mean area of heavy precipitation features, A_m, for interannual variability. The contour shows the 90th percentile of the climatological C and crosses indicate whether correlations are statistically significant.

sections/result_1/spatial_preference2.pdf

Figure 3. Scatter plot of monthly anomalies in area fraction of heavy precipitation, A_f, and the mean area of heavy precipitation features, A_m, colored by the zonal proximity of heavy precipitation to the longitude 180° E in the central pacific, C_z, for GPCP observations (a). Boxplot of the correlations between A_f and A_m and partial correlations of C_z and the proximity of heavy precipitation to the equator, C_m, with A_m outside the influence of A_f for the CMIP6 ensemble (b). The fraction of CMIP models with statistically significant correlations is indicated below each box, and the GPCP (star) and high-resolution GCM (diamond) correlations are shown in lighter colors if not statistically significant.

We now consider how large-scale clustering of heavy precipitation changes under climate change. **?** noted that large-scale clustering increases as the climate warms in projections of climate change by the CMIP5 ensemble. Figure **??**a shows that this is also true for CMIP6; all models project an increase in A_m with warming to varying degrees. However, there is a wide spread in climatological A_m and wide spread in climatological increase in A_m across the ensemble, suggesting the degree of large-scale clustering and the change in large-scale clustering with warming is poorly constrained in the models.

Given the climatologically fixed A_f in this framework, changes in the mean area of precipitation features, A_m, with warming are driven entirely by a spatial reorganization of convection to larger features. The present analysis evaluates whether the spatial patterns associated with a high degree of clustering of precipitation in interannual variability may also be relevant to the redistribution of heavy precipitation causing increased clustering under warming. Indeed, all but one model show a reduction in C_m with warming, indicating a contraction of heavy precipitation towards the equator (Figure **??**b). Further, all models contract heavy precipitation towards the hydrological equator, or "ITCZ center", which is defined here as the latitude of highest specific humidity at 700 hPa as a function of longitude and time in months (Figure **??**c). One possible interpretation of this is that a narrowing of the ITCZ provides a mechanism for the overall increase in clustering with warming. However, we note that the change in C_m with warming is uncorrelated with the change in A_m across the CMIP6 ensemble; models exhibiting stronger ITCZ narrowing with warming do not show stronger increases in large-scale clustering of precipitation. On the other hand, there is a significant correlation between increases in mean area of precipitation features, A_m, and changes in C_z across the CMIP6 ensemble. That is, models that show a greater clustering with warming also show a more zonal shift of heavy precipitation to the central Pacific (note that the zonal and meridional contractions are somewhat anticorrelated, as also identified by **?**).

Going beyond the simple distance metrics, Figure **??** regresses the projected increase in frequency of occurrence of heavy precipitation onto the projected increase in A_m across the CMIP ensemble. This reveals a spatial pattern of precipitation changes with several similarities to the pattern for interannual variability shown in Figure **??**. However, an important distinction is that, for changes with warming, the redistribution of heavy precipitation is a conserved property, due to the climatologically fixed A_f. Similarities between the regression patterns include a regression coefficient largest in the central Pacific close to the equator, and a redistribution of precipitation away from the maritime continent, Amazon, and Atlantic. While under interannual variability heavy precipitation shifts southward in the Pacific for highly clustered states, the changes with warming show a northward shift of heavy precipitation in the Pacific.

We note that the spatial patterns associated with a climatologically high degree of clustering of heavy precipitation across the CMIP6 ensemble are rather different from those of internal variability and changes with warming (Figure S6c in the supporting information). Models with high climatological values of A_m tend to have more convection in the warm pool, over tropical continents, and at the edges of the northern and southern convergence zones over the Pacific Ocean. These relationships cannot be summarized by a single value of either C_z or C_m. Rather, we find that high climatological values of A_m are associated with high month-to-month variability in A_f. This indicates that high spatial clustering also corresponds to high clustering in time, with some days producing a large amount of heavy precipitation across the tropics and other days producing much less.

sections/result_1/spatial_preference3.pdf

Figure 4. Scatter plot of change in climatological mean area of heavy precipitation features, A_m, with change in climatological mean distance of heavy precipitation to the central pacific, C_z, (a) and change in mean heavy precipitation proximity to the equator, C_m (b). Boxplot of change in climatological mean distance to the hydrological equator, C_{heq}, (c) where the hydrological equator is defined as the latitude of highest specific humidity at 700 hPa as a function of longitude and time in months. All quantities are normalized by the tropical surface temperature warming from the historical to the SSP585 scenario simulation period in CMIP6 models.

Figure 5. Increase in frequency of occurrence of heavy precipitation, C, regressed onto increase in A_m per kelvin tropical warming from the historical to the SSP585 scenario simulation period across the CMIP6 ensemble. Contour shows the ensemble-mean 90th percentile of C in the historical period and crosses indicate whether correlations are statistically significant.

In summary, the spatial patterns of heavy precipitation associated with highly clustered states vary across timescales, but there are important common threads. In both internal variability and for changes with warming, higher clustering as measured by A_m is associated with more heavy precipitation in the central equatorial Pacific. In particular, models with stronger increases in large-scale clustering of precipitation under warming also exhibit greater zonal shifts in convection to the central Pacific. This potentially suggests the Walker circulation, and the East-West SST gradient in the Pacific, as an important control on the magnitude of changes in large-scale clustering of precipitation with warming. We next investigate the relationships between SST changes and changes in A_m in both internal variability and under climate change.